Computational Fluid Dynamics Study to Access the Effect of non-Newtonian Fluid Flow Variables on Drilling Mud in Annular Oil Well

Fatemeh Saberi* and **Sara Vashaghian**, University of North Dakota, Grand Forks, United State; **Pourya Asoude**, Shahid Beheshti University, Tehran, Iran; **Ahmed E. Radwan**, Jagiellonian University, Kraków, Poland

Abstract

During the drilling operations, a non-Newtonian fluid type comes out of the space between the drill bit and the well diameter. After the drilling operation, to strengthen the well and prepare an insulating membrane around the well, a metal shell with a diameter smaller than the diameter of the well is installed at a distance from the well and often outside the center. In the well, the fluid inside the mud wells is directed from the drilling to the outside. The main problem that has attracted the attention of researchers is the investigation and calculation of the physics of fluid flow inside these circular spaces. Studying flow physics in laboratories is very expensive, which increases the cost of product design and the product's final price. The movement of drilling mud between the drill bit and the well can be simulated as a non-Newtonian fluid flow inside eccentric tubes where the inner tube is rotating, using computational fluid dynamics. This study aims to numerically simulate the parameters affecting the physics of drilling mud fluid (non-Newtonian fluid) in the space between two non-central cylinders. The flow is incompressible, and with increasing rotation speed, the greater penetration of the boundary layer into the shear stress ring penetrates more inside. It causes the non-Newtonian viscosity values to decrease. It penetrates the mainstream and decreases the non-Newtonian viscosity, more significant than the rotational velocity effect.

Introduction

Engineers in the oil and gas industry usually face non-Newtonian fluid flow in drilling activities. In the context of non-Newtonian fluid, the behavior of drilling fluids is significantly influenced by their rheological properties, which dictate how these fluids respond to applied stress. Non-Newtonian fluids, unlike Newtonian fluids, exhibit a change in viscosity with varying shear rates, making their flow characteristics complex and highly dependent on the specific conditions encountered during drilling operations. The drilling fluid plays a crucial role in maintaining wellbore stability and optimizing reservoir recovery, a function that can be understood through its non-Newtonian behavior. Its effects can be both beneficial and detrimental, depending on the fluid's properties and the specific well conditions. Drilling fluid helps to support the wellbore walls, preventing collapse and maintaining stability, while also inhibiting shale swelling and dispersion, which can lead to wellbore instability (Goshtasbi et al. 2013; Abbasi et al. 2024; Barati et al. 2023; Bina et al. 2020; Bina et al. 2012; Elyasi et al. 2023; Hashemi et al. 2024; Saberi et al. 2024a). Additionally, the fluid helps to remove cuttings and debris from the wellbore, reducing the risk of wellbore instability caused by accumulated cuttings. However, drilling fluid can also cause formation damage, which can reduce reservoir permeability and affect recovery (Makarian et al. 2023a;

Improved Oil and Gas Recovery

DOI: 10.14800/IOGR.1292

Received July 6, 2024; revised August 17, 2024; accepted September 19, 2024.

*Corresponding author: fatemeh.saberi@ndus.edu

Larki et al. 2024). The fluid's invasion into the formation can lead to clay swelling and dispersion, emulsion formation, and precipitation of solids, all of which can reduce permeability. Furthermore, fluid loss can occur, reducing the reservoir's hydrocarbon saturation and leading to decreased hydrocarbon recovery. There are some ways to recognize hydrocarbon saturation and evaluate the behaviour of fluids through porous media such rock physics, which fluids with some properties such as seismic velocities and density are investigated (Makarian et al. 2023b).

To optimize drilling fluid performance, it is essential to select a fluid formulation that aligns with the non-Newtonian flow characteristics required for the specific well conditions. This involves adjusting the fluid's rheological properties, such as yield point, plastic viscosity, and gel strength using additives and control measures. Strategies like lost circulation materials (LCMs) and fluid loss additives can effectively manage fluid invasion and minimize formation damage, ensuring sustained drilling fluid effectiveness throughout the drilling process. Therefore, understanding these non-Newtonian flow variables of drilling fluids is therefore critical for enhancing wellbore stability, mitigating risks, and maximizing reservoir recovery through optimized drilling performance.

Salubi et al. (2022) and Liu et al. (2022) investigated the physical characteristics of non-Newtonian fluid flow velocity in annular channels, and employed an aqueous solution of sodium carboxymethyl cellulose (CMC, a weakly elastic shear-thinning polymer) to model drilling mud in the interannual space. Moreover, Deshmukh and Dewangan (2022) utilized three shear-thinning aqueous solutions of CMC, xanthan gum, and Laponite/CMC mixture. In the last test he carried out, the concentric ring was 2.5 times larger than the previous two studies in spite of the same diameter ratio. The agreement between the CMC results indicated that the flow characteristics are similar to the Newtonian fluid in the laminar flow regime. Brethouwer (2023) for air and light and Dai et al. (2023), and Deshmukh and Dewangan (2022) studied fluid flow physics in the concentric computational domain for Newtonian and non-Newtonian fluids experimentally. The rotation speed decreases rapidly from the rotating inner cylinder in most of the core region, and the rotation penetration decreases as the Reynolds number increases. The rotation creates a uniform axial mean flow and increases the flow resistance. Nino et al. (2022) shows that the non-Newtonian fluid's rotation increases the crossflow components' turbulence intensity. As described by Vipulanandan and Mohammed (2020), at the beginning of the drilling process, the drilling mud (initial penetration 1) penetrates rapidly into the formation as soon as drilling starts. Penetration and deposition of solid mud particles in the porous medium cause an internal mud cake to form within a few minutes. After that, most solid mud particles settle on the well wall, forming an external mud cake. This mud cake controls the penetration of the drilling fluid into the formation (Mirhashemi et al. 2022; Vipulanandan and Mohammed 2020).

There are laboratory and analytical methods to determine the radius of drilling mud invasion. In laboratory methods, the radius of penetration is determined by measuring the electrical resistance of the formation (Gamal et al. 2021). Dewan and Chenevert conducted experiments based on water-based drilling mud to study mud cake growth (Chenevert and Dewan 2001). They designed an experiment to determine acceptable mud cake parameters and proposed a mathematical model to predict cake thickness and permeability using parameters such as cake mass, fluid density. Some researchers strived to numerically simulate the sensitivity analysis with the same theory. They developed and expanded the properties of mud cake and rock, seepage flow, and mud cake (Wu et al. 2004; Sepehrnoori et al. 2005). Li et al. (2022) developed a hydro mechanical model by the effect of time-dependent mud cake to evaluate the impact of water-based drilling fluid on properties of mud cake and wellbore stability. Carollo et al. simulated the equations of motion with a numerical method (finite difference technique). Using dipole coordinates. They obtained the velocity characteristics for Newtonian fluid flow in eccentric annular geometries (Carollo et al 2023; Saberi et al. 2024b; Saberi and Hosseini-Barzi, 2024; Saberi et al. 2023; Vashaghian et al. 2024; Zanjirabadi et al. 2024). Puranik et al. (2023) considered the heat transfer effect on peristaltic motion of Newtonian fluid flow. By implementing a perturbation method, they achieved an approximate solution for velocity and temperature for such and evaluated the pressure at constant flow rate.

Ershadnia et al. (2020) developed a physical-based and data-driven solution for laminar flow of non-Newtonian fluids in rotating annular media. They investigated the Importance of coaxial rotation of inner cylinder on overall pressure loss while focusing on the dynamics of pressure loss ratio. Using a finite difference numerical solution,

Miao et al. (2023) studied the laminar flow of non-Newtonian fluids in the ducts of a section. They investigated the volume flow rate in a pressure gradient.

In this study, the frictional behavior of non-Newtonian fluids in drilling operations was done using Computational Fluid Dynamics (CFD) approach. Numerical fluid flow analysis in an eccentric ring, with Newtonian and non-Newtonian fluids, helps understand the physics of the fully developed turbulent fluid flow. Due to the complex geometry of an annular space, CFD simulation studies of Newtonian and non-Newtonian power-law fluid flow can greatly contribute to accurate analysis. This project investigated the effect of parameters affecting fluid flow physics, such as fluid flow rate and wall rotation speed.

Simulation Method

In this study, a fully developed turbulent flow simulation of Newtonian and non-Newtonian fluids in drilling operations have been carried out using FLUENT, a commercial computational fluid dynamics (CFD) code developed by ANSYS. These solvers are based on the finite volume method; the flow domain is discretized into a limited set of volumes or control cells. In CFD models, each governing equation is integrated numerically on a control volume, so the relevant quantity (mass, momentum, energy, etc.) is solved and obtained on each cell. Fluent provides a measure of control by providing user-selectable discretization strategies and alternative solutions. Care must be taken in choosing the discretization and solution methods considering the complex fluid flow in the annular channel.

Governing Equation. The differential equations governing the flow of non-Newtonian fluids are based on the Navier-Stokes equation and are defined as follows (**Eqs. 1** through **2**),

$$\frac{\partial \rho}{\partial t} + \frac{\partial}{\partial x_i}(\rho u_i) = 0, \quad (1)$$

$$\frac{\partial}{\partial t}\left(\rho u_j\right) + \frac{\partial}{\partial x_i}\partial u_i u_j = -\frac{\partial P}{\partial x_j} + \frac{\partial}{\partial x_i}(\mu + \mu_t)\left(\frac{\partial u_i}{\partial x_j} + \frac{\partial u_j}{\partial x_i}\right) + \rho g_i \quad (2)$$

The Power Law governs the viscosity is defined as follows (**Eq. 3**),

$$\mu K \times \gamma^{n-1} \quad (3)$$

where n =0.75 which is the power law index (flow behavior index: n=1, Newtonian; and n<1, Non-Newtonian flow); K is consistency index, equal to 0.044; γ is local shear rate.

FLUENT software offers several turbulent models to solve problems; the robust and reasonable accuracy of the turbulence model explains its popularity in industrial flow and heat transfer simulations. is a semi-empirical model, and the extraction of model equations is based on phenomenological considerations and empiricism. This model includes the standard equations of turbulence kinetic energy transfer (k) and its dissipation rate (ε). The equation of kinetic energy of disturbance k and its dissipation rate ε is obtained from the following transfer equations (**Eqs. 4** and **5**),

$$\frac{\partial}{\partial t}(\rho k) + \frac{\partial}{\partial x_i}(\rho k U_i) = \frac{\partial}{\partial x_j}\left[\left(\mu + \frac{\mu_t}{\sigma_k}\right)\frac{\partial k}{\partial x_j}\right] + G_k + G_b - \rho\epsilon - Y_M + S_k, \quad (4)$$

$$\frac{\partial}{\partial t}(\rho \varepsilon) + \frac{\partial}{\partial x_j}(\rho \varepsilon U_i) = \frac{\partial}{\partial x_j}\left[\left(\mu + \frac{\mu_t}{\sigma_k}\right)\frac{\partial \varepsilon}{\partial x_j}\right] + C_\varepsilon \frac{\epsilon}{k}(G_k + C_{3\epsilon}G_b) - C_{2\epsilon\rho}\frac{\epsilon^2}{k} + S_\varepsilon \quad (5)$$

These equations represent the kinetic energy production of fluid turbulence caused by average velocity gradients. C_{1e}, C_{2e} and C_{3e} are constants. Furthermore, σ_k and σ_ε are the turbulent Prandtl number for k and ε, respectively. Furthermore, S_k and S_e are user-defined source terms. The turbulent viscosity μ_t is computed as follows (**Eq. 6**),

$$\mu_t = \rho C_\mu \frac{k^2}{\epsilon}, \quad (6)$$

where C_k is constant. The default values for the constants C_{1e}, C_{2e}, C_k, S_k and S_e. are 1.44, 1.92, 0.09, 1.0, and 1.3, respectively. These default values work well for various wall-bounded and free-shear flows.

In the current research, the governing equations of three-dimensional turbulent flow are addressed by employing the finite volume discretization technique, in which control volume cells are employed for the velocity components by the SIMPLE method. The pressure correction relation, derived from the continuity equation, is figured out to gain a pressure correction field utilized in order to update the velocity and pressure fields. These guessed fields are gradually improved by iteration until convergence to be gained for the updated fields.

The discrete conservation equations are addressed iteratively so that they gain convergence. For instance, when the changes in the solution variables (residuals) from one iteration to the next are within the convergence criteria, being set to keep the residual velocity and x-y-z at appropriate convergence was gained utilizing under-relaxation factors from 0.2 to 0.3 and 0.5 to 0.7 for pressure and momentum, respectively.

Model Geometry and Grid Generation. GAMBIT software was used to generate geometry and grid. Different types of cells can be used for a three-dimensional computing domain, including hexagonal, tetrahedral, pyramidal, wedge, and hybrid cells. The grid independence and numerical results for three cases have been studied (**Figures 1** to **3**)

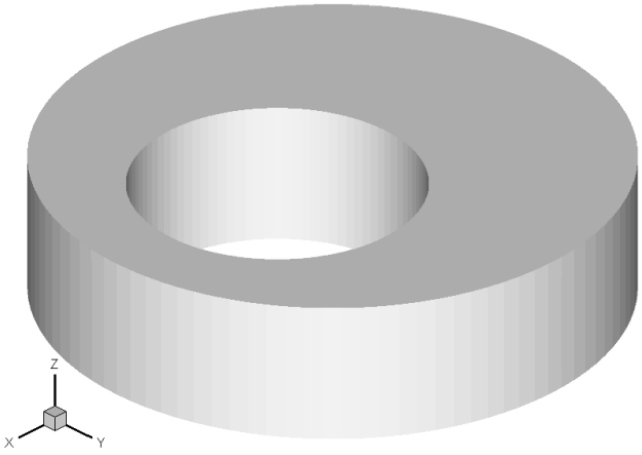

Figure 1—Eccentric annuli geometry.

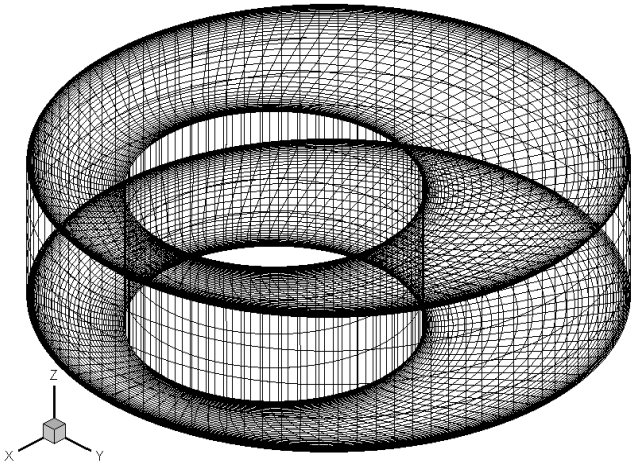

Figure 2—Eccentric annuli mesh distributions.

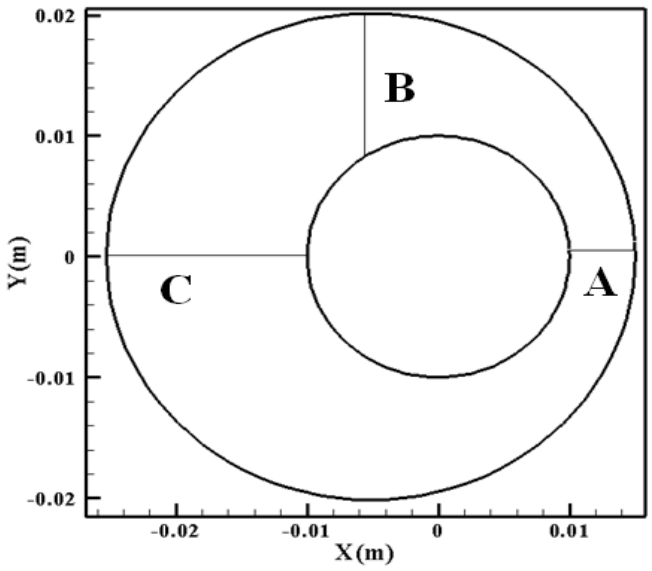

Figure 3—Line A, B, C in eccentric annuli geometry plane.

For the boundary conditions, the mass flow rate (1.3, 2.6, and 5.2 kg/s) and the rotation speed of the inner wall (0, 300, and 600 rpm) were considered. The simulations were performed under steady-state conditions, and fluid was considered incompressible. Isothermal conditions are assumed. The boundary condition of non-slip was considered on the inner and outer walls.

Results and Discussion

Tangential Velocity. The first simulation studies the tangential velocity effect of the inner surface. We changed the boundary condition of the inner surface to various speeds to examine the effect of the rotation of the inner surface(cylinder) on axial velocity, laminar viscosity, turbulent viscosity, and turbulent kinetic energy profiles at 0, 300 and 600 rpm in the positive z direction(counter clockwise). A, B, and C lines are assumed to plot different profiles in specific surfaces in essential regions to fully understand the behavior of be examined variables.

Axial Velocity. **Figure 4** shows the axial velocity counters in 0, 300 and 600 rpm rotational velocity. With the increase in rotational velocity in Q=2.6, the maximum of the counters is moved and the velocity profiles are not symmetric anymore. Moreover, the profile is more and more homogenous. That means fluid moves more homogeneously in the z direction, and less axial velocity gradient is observed. It is essential to mention that in all of the counters, the mass flux is maintained at 2.6 kg/s. The effects caused by the boundary layer decrease in A, B and C, respectively, due to the increased distance between the two circular surfaces. Therefore, when the rotational speed is zero, the axial velocity in section A is lower than B and C.

Nevertheless, with the increase of rotational speed due to the reduction of the effect of the boundary layer in this area, we see an increase in the maximum speed in this area and, vice versa, a decrease in the maximum speed in the other three lines, B and C. **Figure 5** shows the axial velocity profiles at A, B, and C lines. As shown in line A, the average axial velocity is increased at a higher tangential velocity. Thus, more fluid is passed through the surface. However, at B and C surfaces, the axial velocity decreased significantly with the increase of tangential velocity. It is also evident that the maximum amount of fluid is passed over the wider region (line C). The results are acceptable as more homogenous profiles will be created with increased axial velocity.

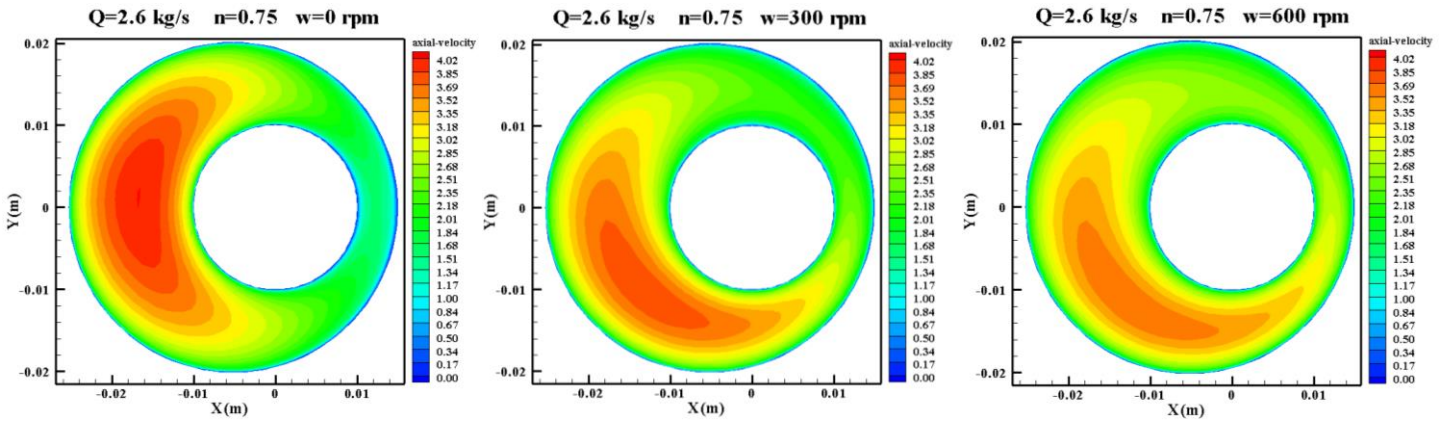

Figure 4—The contour of axial velocity in eccentric annuli (rotational velocity effect).

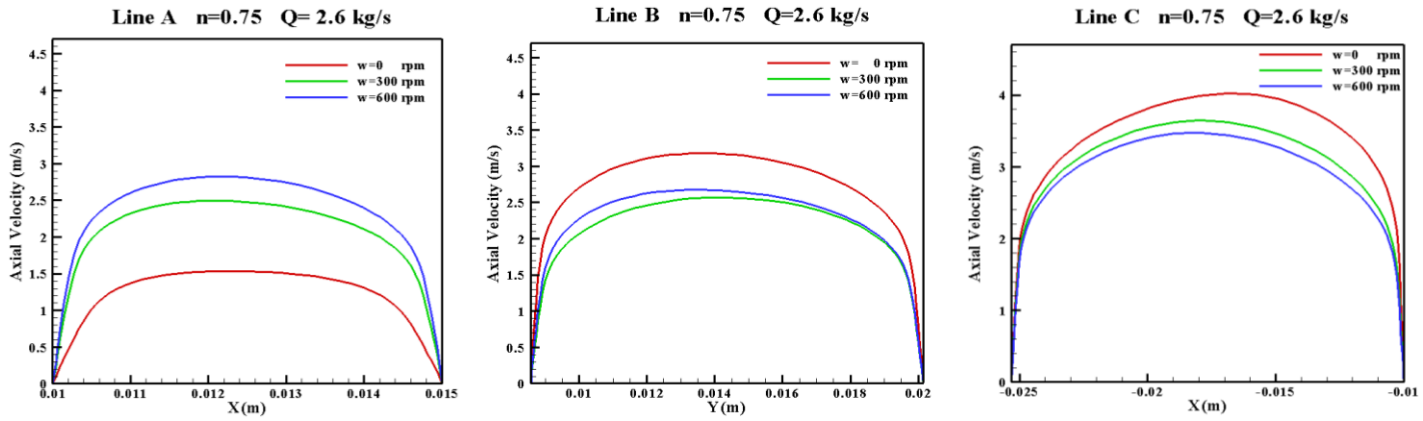

Figure 5—The axial velocity profile in lines A, B and C in eccentric annuli (rotational velocity effect).

Laminar Viscosity. Laminar viscosity contours and profiles are shown in **Figures 6** and **7**, respectively. Figure 6 shows that the laminar viscosity contours are smoothed with increased rotational velocity. In other words, as rotational velocity increases, a more shear rate is applied to the bulk fluid. Thus the non-Newtonian fluid will have lower viscosity and less rigid changes are observed in the laminar viscosity counters. The same has happened in the laminar viscosity profiles at the A, B, and C regions shown in Figure 7. In all cases, the laminar viscosity is changed according to the change in axial velocity and, thus, shear rate profiles. The maximum of the plots, in which we observe maximum velocity, is shifted in all cases because of the shift in velocity profiles. For example, at line C, the rotational velocity affects the axial velocity profile and shifts it to be higher at bigger x values. This results in a significant decrease in laminar viscosity in these regions. So the maximum is shifted to more significant x values.

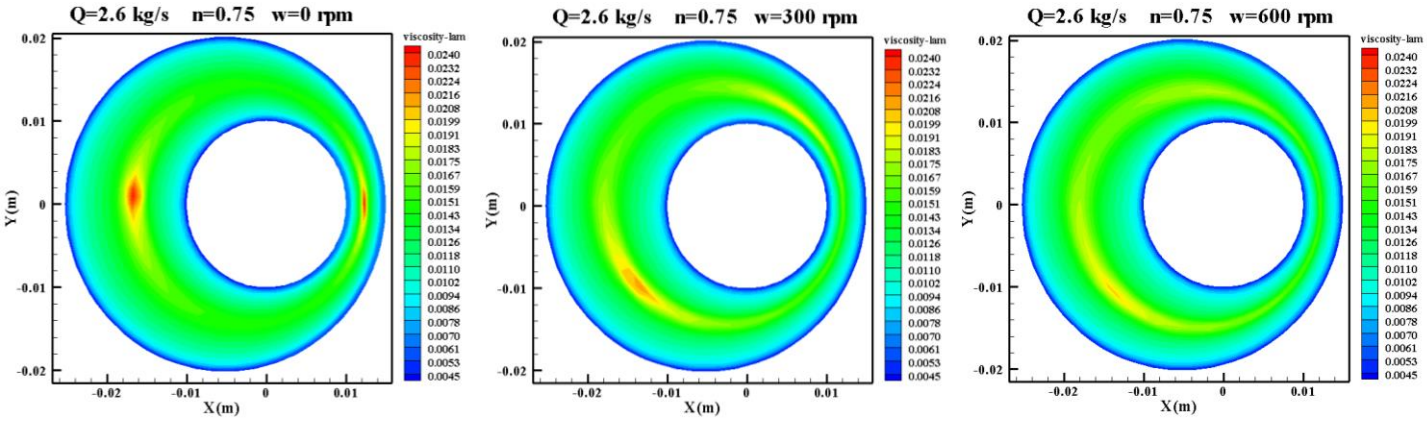

Figure 6—The contour of laminar viscosity in eccentric annuli (rotational velocity effect).

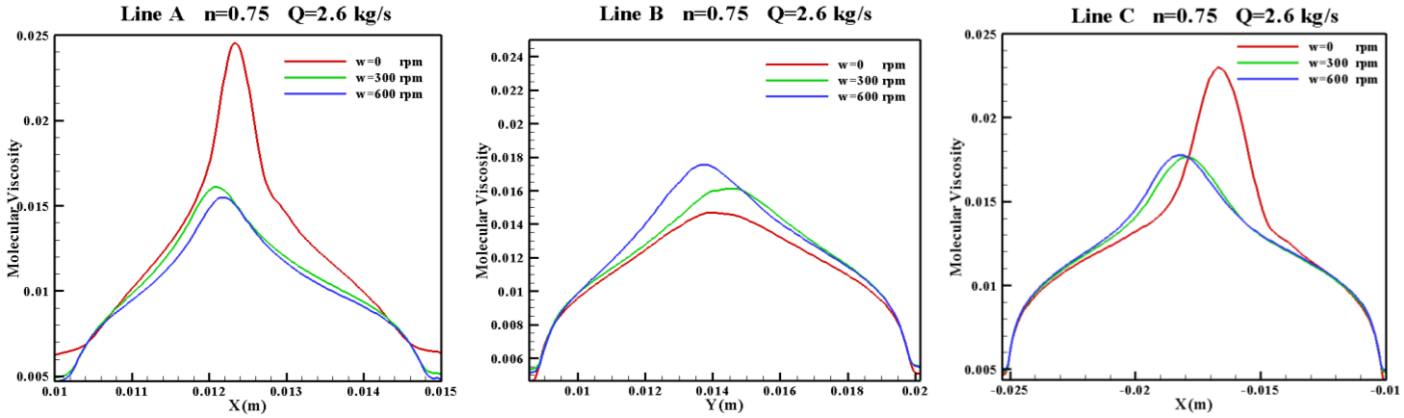

Figure 7—The laminar viscosity profile in line A, B and C in eccentric annuli (rotational velocity effect).

***Turbulent Viscosity*.** Turbulent velocity characterizes the chaotic and irregular fluid motion that defines turbulent flow, leading to significant fluctuations in velocity and pressure. Unlike the smooth layers observed in laminar flow, turbulent flow exhibits non-uniform axial velocity profiles, indicating varying levels of resistance and energy transfer along the flow direction. The presence of dual velocity maxima offers regions of increased turbulence intensity and flow acceleration driven by pressure differentials. Furthermore, while laminar viscosity refers to the fluid's internal resistance under laminar conditions, turbulent flow complicates this concept as effective viscosity, influenced by turbulence, becomes variable and is often described as turbulent or eddy viscosity. This interplay of axial velocity and viscosity highlights the intricate dynamics of turbulent flow, necessitating a detailed analysis to understand the overall flow characteristics thoroughly. Moreover, in the specific context of computational fluid dynamics in drilling operations, turbulent velocity refers to the disorderly and tumultuous movement of fluid particles within the annular space between non-central cylinders. **Figures 8** and **9** manifest the turbulent counters and profiles, respectively. Turbulent flow is generally difficult to explain. As we can see, there are two maximums in the contours and profiles.

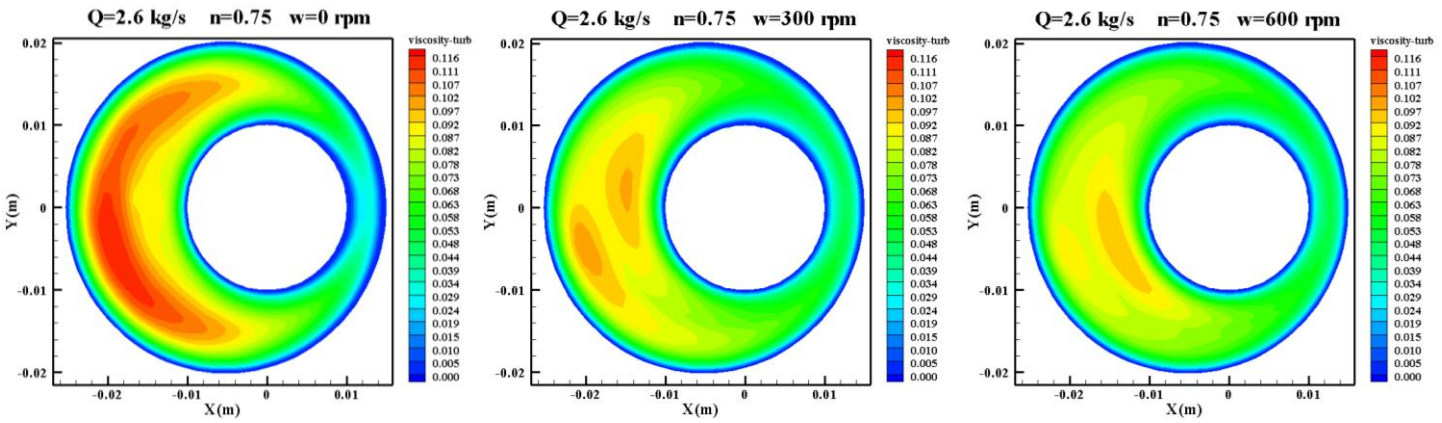

Figure 8—The contour of turbulent viscosity in eccentric annuli (rotational velocity effect).

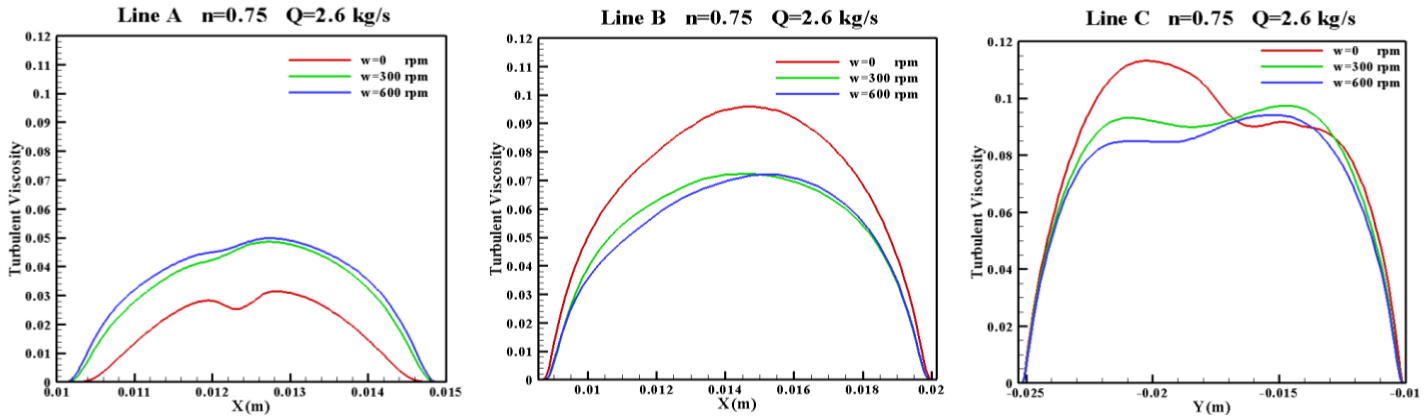

Figure 9—The turbulent viscosity profile in Line A, B and C, in eccentric annuli (rotational velocity effect).

***Turbulent Kinetic Energy*. Figure 10** displays the contour of turbulent kinetic energy, highlighting how it is distributed in the annuli when the inner surface rotates at different speeds. Notably, the depiction shows how the intensity of turbulent kinetic energy evolves as the rotational velocity of the inner surface escalates. Specifically, as the rotational velocity increases, the distribution of turbulent kinetic energy becomes more pronounced, with higher energy levels observed near the rotating inner surface. The scale depicted in the figure, which corresponds to turbulent kinetic energy, indicates that at higher rotational speeds, the energy values increase significantly, indicative of intensified turbulence. These concepts are important for recognizing regions of high and low turbulence utilized for optimizing drilling operations by ensuring efficient fluid flow and minimizing wear on equipment.

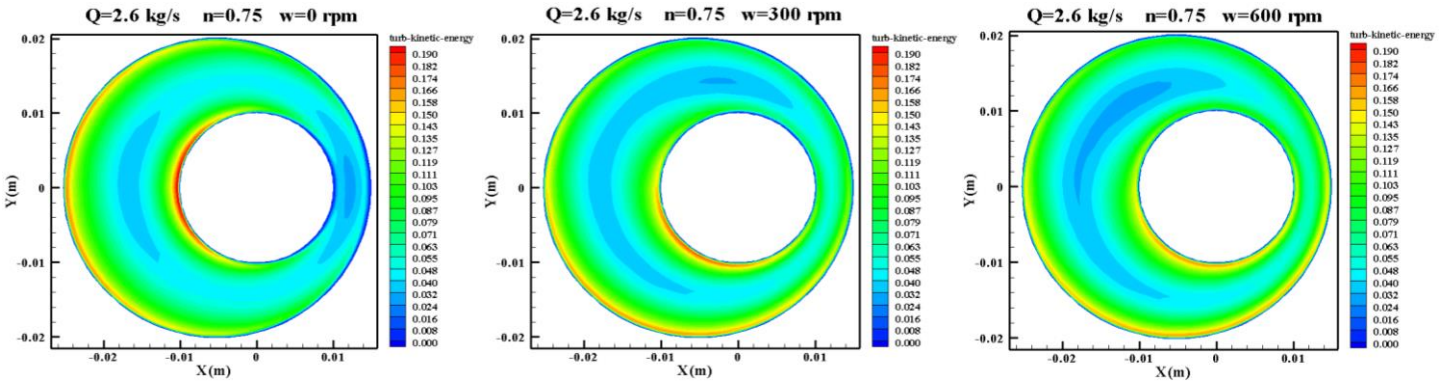

Figure 10—The contour of turbulent kinetic energy in eccentric annuli (rotational velocity effect).

Figure 11 reveals an array of essential information analysis by providing the turbulent kinetic energy profiles along three different lines, denoted as A, B, and C, traversing the eccentric annular region. These profiles provide a detailed view of how turbulent kinetic energy varies at specific radial positions. Based on the figures, line A, positioned closest to the inner rotating surface, shows the highest difference turbulent kinetic energy with speed variations because of the direct influence of rotational velocity. The visualization indicates that the red line, corresponding to the lowest rotational speed, exhibits the least energy, while the green and blue lines, associated with higher speeds, demonstrate progressively heightened energy levels. The significant distance between these lines indicates a strong influence of rotational speed in proximity to the inner surface. Moving on to Line B, situated at a mid-radial location, a moderate distribution of turbulent kinetic energy is observed. The red line shows higher energy levels compared to other lines, but the differences are less pronounced than in Line A, reflecting the diminishing influence of rotational velocity with increasing radial distance. The reduced distance between the lines shows a more uniform energy distribution. Lastly, Line C, positioned near the outer stationary surface, shows the lowest levels of turbulent kinetic energy. The red, green, and blue lines converge more closely, indicating minimal influence of rotational velocity at this position, with the minimal separation between the lines suggesting a nearly uniform energy distribution, irrespective of the rotational speed.

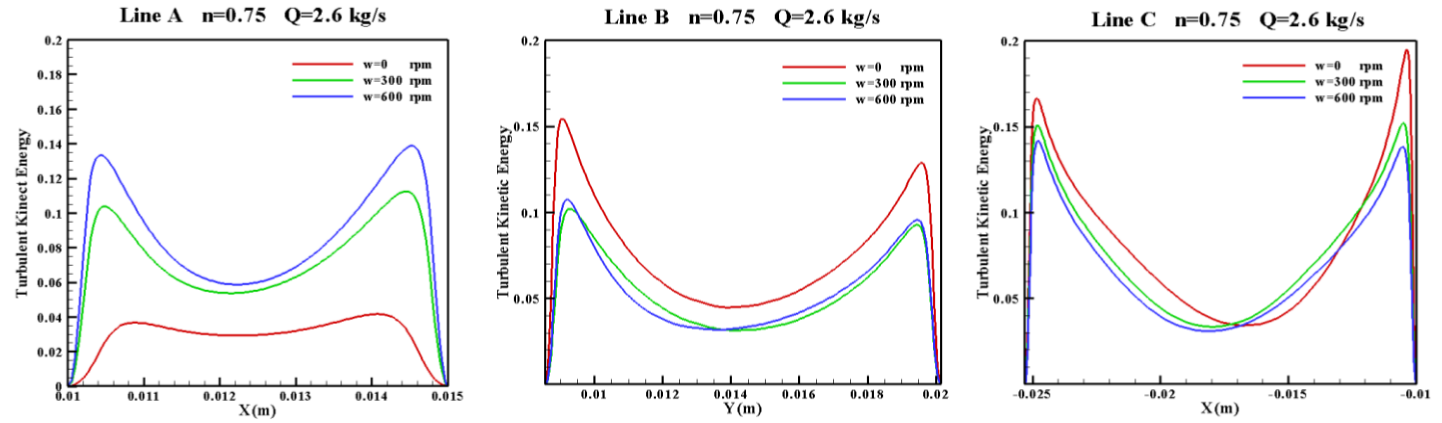

Figure 11—The turbulent kinetic energy profile in lines A, B and C, in eccentric annuli (rotational velocity effect).

Mass Flux. The second simulation studies the mass flux effect of the bulk fluid. We changed the volume flux amount of the bulk fluid at the same tangential speed (300rpm) to examine the effect of total mass flux on axial velocity, laminar viscosity, turbulent viscosity, and turbulent kinetic energy profiles at 1.3, 2.6 and 5.2 kg/s mass flux of bulk fluid. A, B, and C lines are assumed to plot different profiles at specific surfaces in essential regions to fully understand the behavior of the examined variables.

Axial Velocity. **Figure 12** shows the axial velocity counters at 1.3, 2.6 and 5.2 kg/s total mass flux of bulk fluid with the inner surface rotating at 300 rpm. With the increase in total mass flux, there is a significant increase in axial velocity, as expected. The critical fact is that the maximum counters and profiles (Figure 10) are placed in the same position, and no shift in contours is observed. However, the profiles are less homogenous and rigid changes are observed in the profiles. That means fluid is moving more at specific wider regions than narrow regions at a higher mass flux (Q=5.2) compared to lower mass fluxes (Q=1.3). **Figure 13** shows the axial velocity profiles at A, B and C lines. As shown in line A, the average axial velocity increases, and more rigid profiles are obtained at higher mass fluxes as mentioned. In line A, since the two walls are close, the effects of the boundary layer between the two walls have grown more. Therefore, with the increase in the speed of the main flow, there is no significant increase in the maximum speed of this area. Similarly, B compared to C.

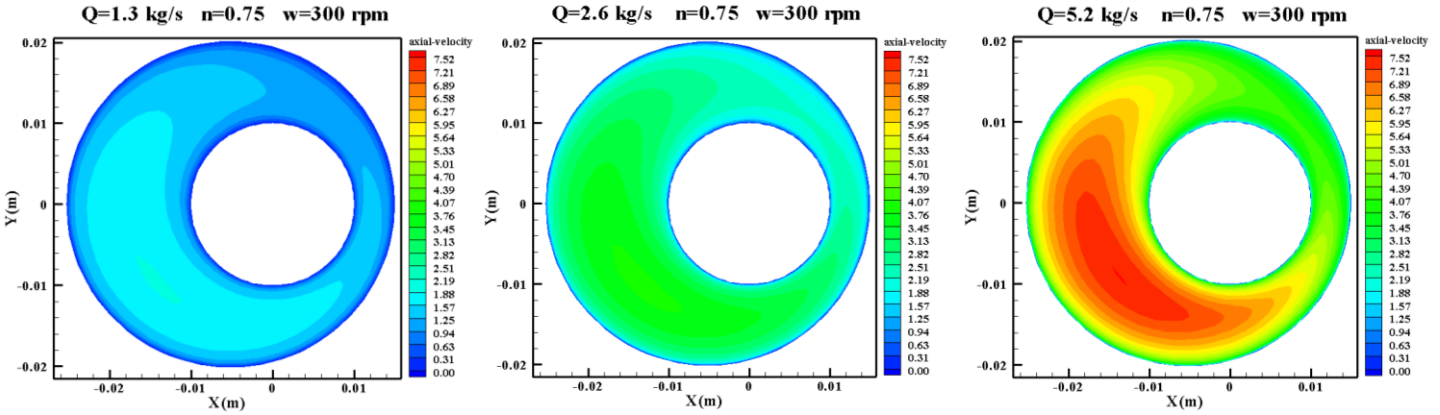

Figure 12—The contour of axial velocity in eccentric annuli (mass flux effect).

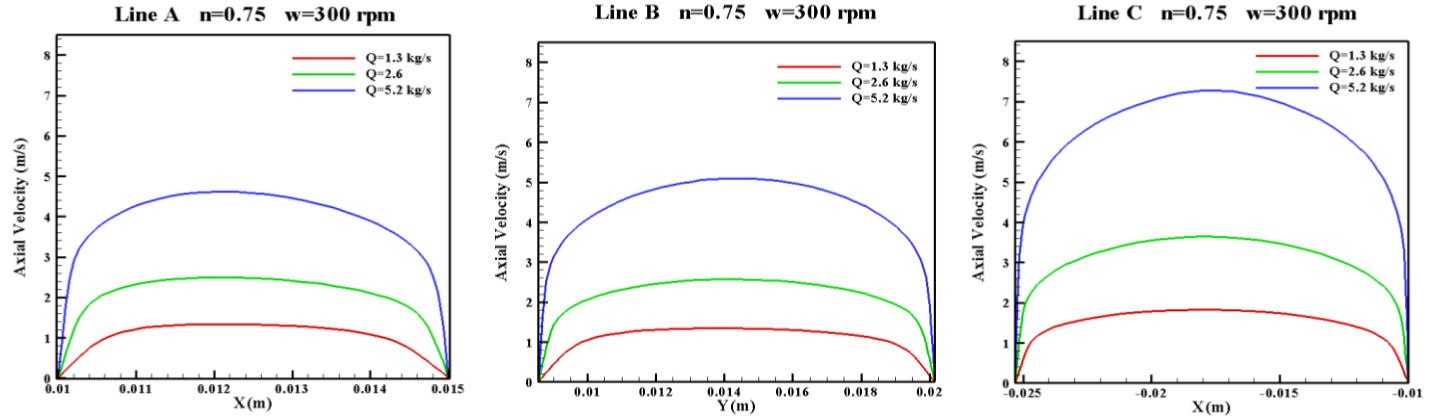

Figure 13—The axial velocity profile in lines A, B, and C in eccentric annuli (mass flux effect).

Laminar Viscosity. Laminar viscosity contours and profiles are shown in **Figures 14** and **15**, respectively. As Figure 14 shows, the laminar viscosity contours are being smoothed with the increase of mass flux. In other words, as mass flux increases, a more shear rate is applied to the bulk fluid. Thus, the non-Newtonian fluid will have lower viscosity and less rigid changes are observed in the laminar viscosity counters. The same has happened in the laminar viscosity profiles at the A, B and C regions shown in Figure 15. In all cases, the laminar viscosity changes according to the change in mass fluxes and thus, shear rate profiles. The maximum of the plots, in which we observe maximum velocity, is maintained in all cases because the tangential velocity is fixed at 300 rpm in all cases.

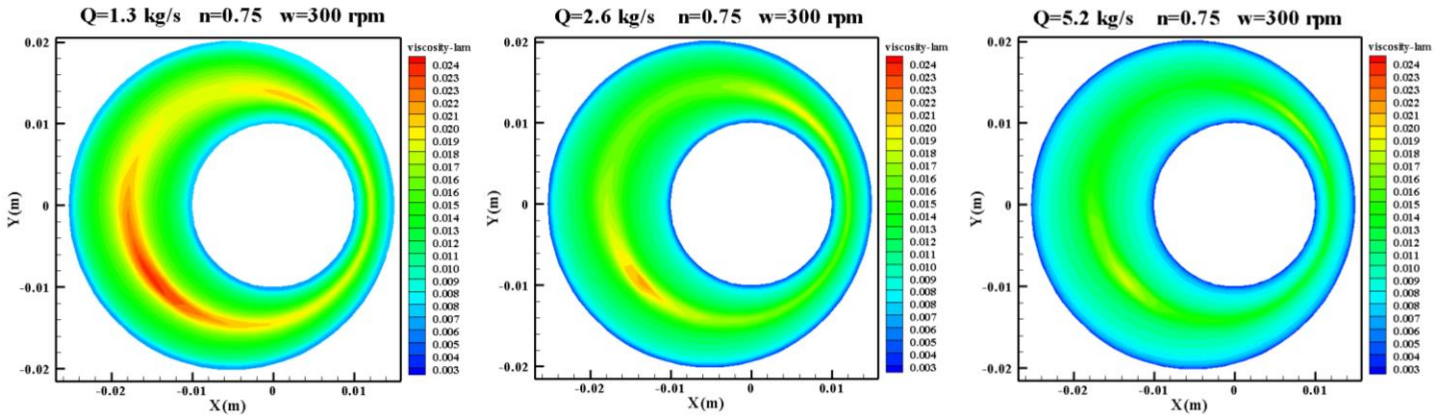

Figure 14—The contour of laminar viscosity in eccentric annuli (mass flux effect).

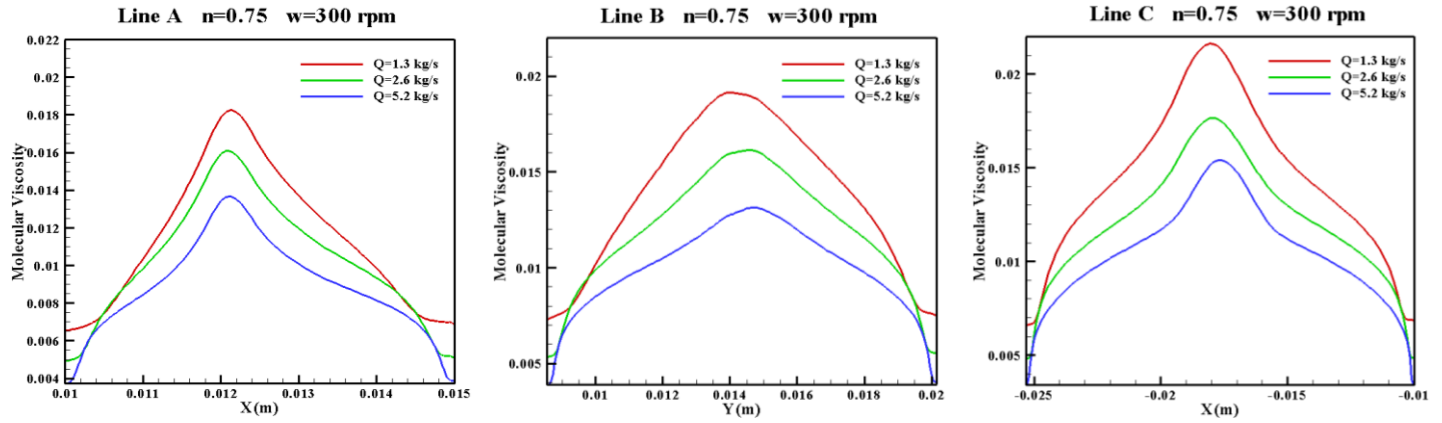

Figure 15—The laminar viscosity profile in Line A, B, and C in eccentric annuli (mass flux effect).

Turbulent Viscosity. Vorticity is a vector measure of the local rotation of fluid elements in a flow field, defined mathematically as the curl of the velocity field. It indicates the tendency of fluid particles to spin, providing crucial insights into the chaotic nature of turbulent flow where regions exhibit varying degrees of rotation. In turbulent flows, the interactions of vortices with high vorticity facilitate energy transfer, leading to kinetic energy dissipation into thermal energy and promoting turbulent mixing. This enhanced mixing improves momentum and mass transfer, which is essential in applications like chemical reactions and heat exchangers. Additionally, vorticity is critical for understanding the development of flow structures, such as boundary layers and wakes, influencing how fluids interact with surfaces and affecting drag and lift forces. **Figures 16** and **17** show the turbulent counters and profiles, respectively. With the increase in the speed of the primary flow, the energy of the vorticity increases, and the viscosity of the turbulence also increases.

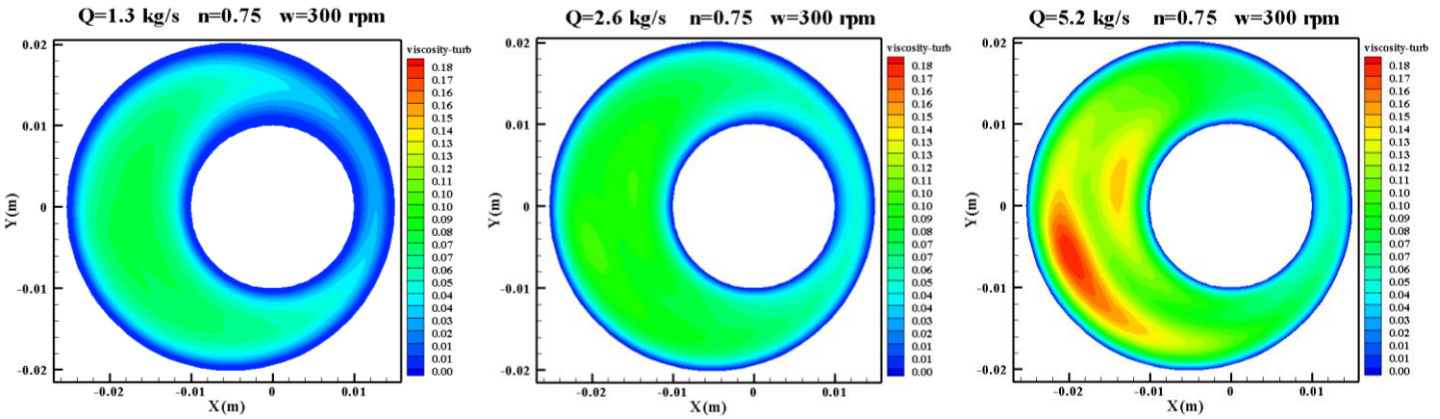

Figure 16—The contour of turbulent viscosity in eccentric annuli (mass flux effect).

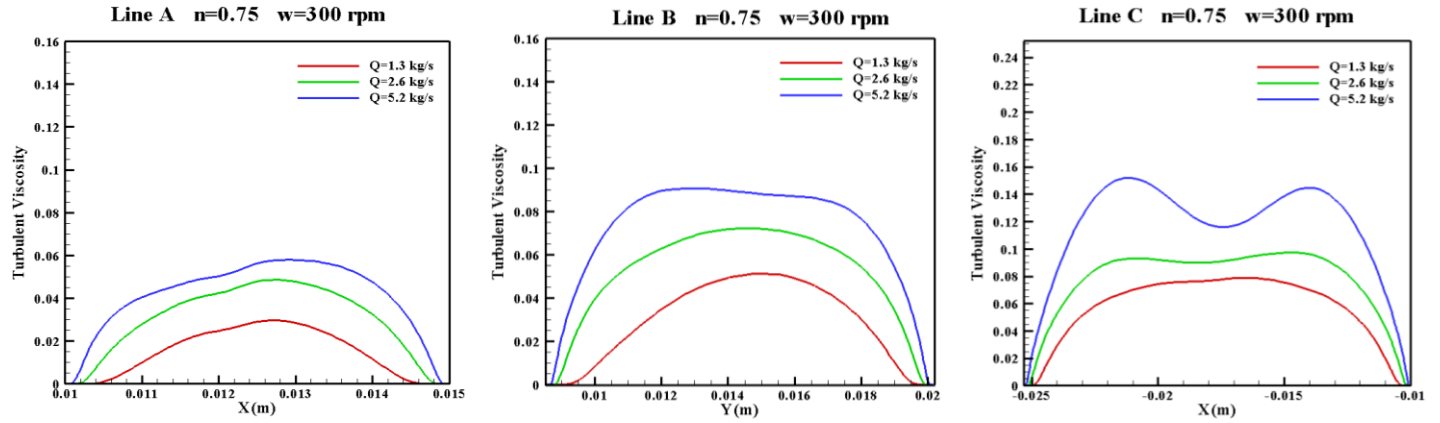

Figure 17—The turbulent viscosity profile in Lines A, B, C in eccentric annuli (mass flux effect).

***Turbulent Kinetic Energy*. Figure 18** shows the contour of turbulent kinetic energy in eccentric annuli, focusing on the effect of mass flux. The contours illustrate how turbulent kinetic energy is distributed within the annuli when the mass flux of the bulk fluid is varied. As the mass flux increases, the turbulent kinetic energy also increases, indicating more intense turbulence. Specifically, at higher mass fluxes (e.g., 5.2 kg/s), the contours show higher energy levels compared to lower mass fluxes (e.g., 1.3 kg/s). This increase in turbulent kinetic energy with mass flux is critical for understanding fluid dynamics, as higher turbulence can enhance mixing and impact the efficiency of drilling operations. The scale of turbulent kinetic energy in the figure helps quantify these changes, showing a clear correlation between mass flux and turbulence intensity.

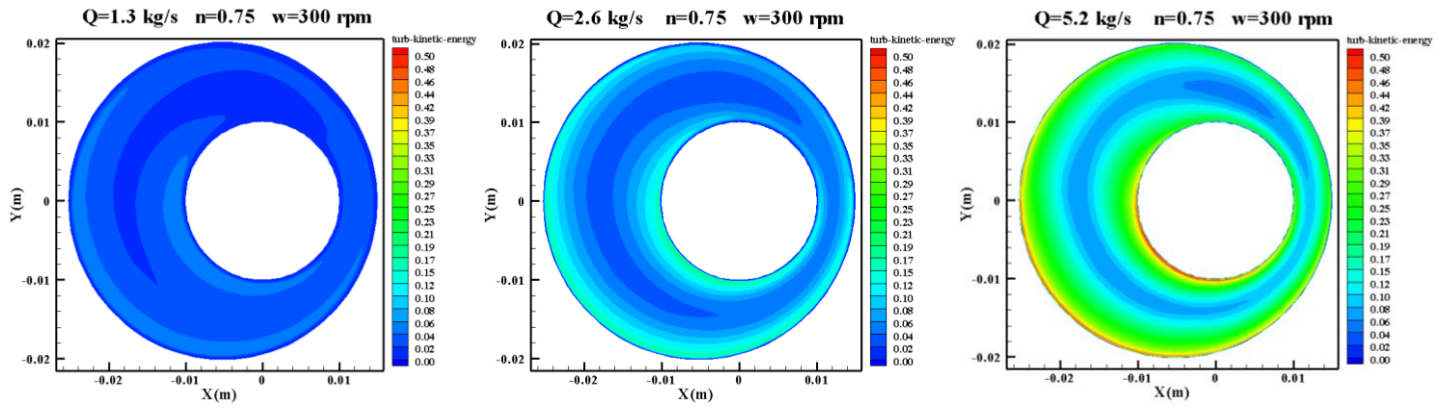

Figure 18—The contour of turbulent kinetic energy in eccentric annuli (mass flux effect).

Figure 19 presents the turbulent kinetic energy profiles along lines A, B, and C within eccentric annuli, focusing on the effect of mass flux. The profiles demonstrate the variation of turbulent kinetic energy corresponding to different mass flux values (Q) of 1.3, 2.6, and 5.2 kg/s. Line C, positioned near the outer stationary surface shows the highest turbulent kinetic energy. The blue line, representing a mass flux of 5.2 kg/s, displays the most significant energy levels, followed by the green line (Q=2.6 kg/s) and the red line (Q=1.3 kg/s). The significant distance between these lines indicates a substantial impact of mass flux on turbulent kinetic energy in proximity to the outer surface. Line B, positioned at a mid-radial location, along with Line A, near the outer stationary surface, show the lower turbulent kinetic energy. Here, the red, green, and blue lines converge more closely, indicating a diminished effect of mass flux. The smallest distance between the lines suggests a nearly uniform distribution of turbulent kinetic energy regardless of mass flux.

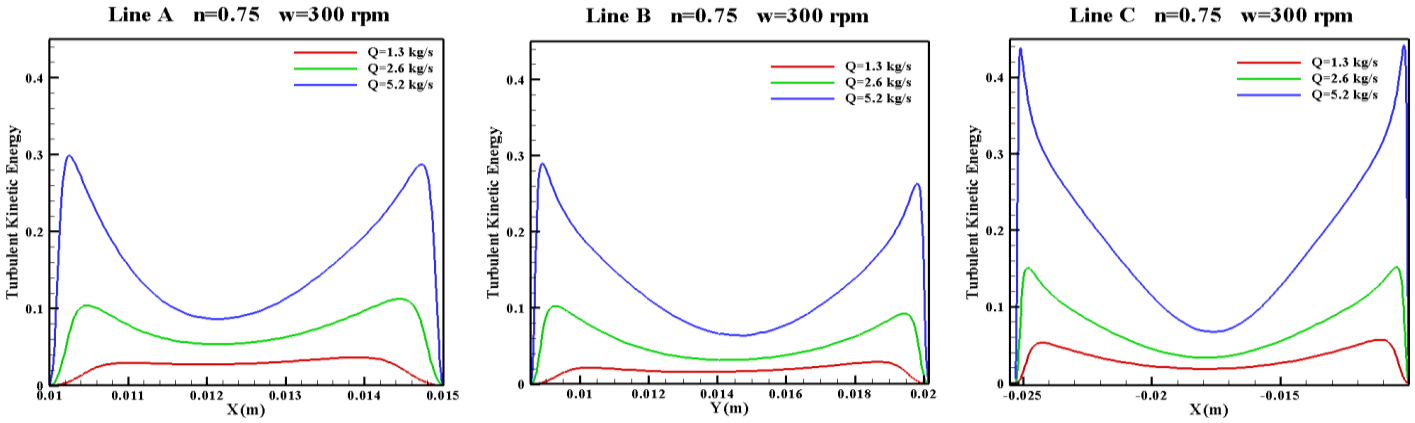

Figure 19—The turbulent kinetic energy profile in line A, B, C in eccentric annuli (mass flux effect).

Conclusions

The objective of this study is to numerically simulate the parameters affecting the physics of drilling mud fluid (non-Newtonian fluid) in the space between the drill bit and the wellbore wall using computational fluid dynamics. The key findings of this study are,

1. Fluid moves more homogeneously in the z direction, and less axial velocity gradient is observed.
2. The axial velocity decreased significantly with the increase of tangential velocity. The results are acceptable as more homogenous profiles will be created with increased axial velocity. As rotational velocity increases, a more shear rate is applied.
3. With the increase in total mass flux, there is a significant increase in axial velocity, as expected
4. With the increase in the speed of the main flow, there is no significant increase in the maximum velocity
5. As mass flux increases, a more shear rate is applied to the bulk fluid. Thus, the non-Newtonian fluid has lower viscosity and less rigid changes are observed in the laminar viscosity.

Nomenclature

ρ	=	density;
u	=	velocity;
t	=	time;
μ	=	viscosity;
μ_t	=	turbulence viscosity;
g	=	gravity;
n	=	power law index;

K = consistency index;
γ = local shear rate;
k = turbulence kinetic energy;
ε = turbulence dissipation rate;
G_k = constant;
G_b = constant;
Y_M = constant;
C_{1e} = constant;
C_{2e} = constant;
C_k = constant;
C_{3e} = constant;
S_k = user-defined source terms;
S_e = user-defined source terms;
σ_k = turbulent Prandtl number for k;
σ_ε = turbulent Prandtl number for ε;

Conflicting Interests

The author(s) declare that they have no conflicting interests.

References

Abbasi, V., Ahmadi, M., Mohtarami, E., et al. 2024. Experimental and Numerical Failure Mechanism Evaluation of Anisotropic Rocks Using Extended Finite Element Method. *Theoretical and Applied Fracture Mechanics* **131*(1)***:104411.

Barati, M. B., Kadkhodaie, A., Soleimani, B., et al. 2023. Determination of Reservoir Parameters of the Upper Part of Dalan Formation Using NMR log and Core in South Pars Oil field. *Journal of Petroleum Research* **33**(1402): 73-83.

Bina, F. A., Sefid, P. J., Porkhial, S., et al. 2012. Estimating the Geothermal Power Potential of the NW-Sabalan Geothermal Field, Iran, by the Volumetric Method. *Proc*., Thirty-Seventh Workshop on Geothermal Reservoir Engineering, Stanford, California, 1-21.

Bina, F. A., Satkin, M., and Shabnavard, A. 2020. Recent Attainments and Regulations in the Field of Geothermal Energy in Iran. Paper presented at the World Geothermal Congress, Reykjavik, Iceland, 1 October.

Brethouwer, G. 2023. Strong Dissimilarity between Heat and Momentum Transfer in Rotating Couette Flows. *Int. J. Heat Mass Transf.* **205**(1): 123920.

Carollo, F. G., Nicosia, A., Palmeri, V., et al. 2023. On the Variation of the Correction Factor of Surface Velocity with the Measurement Vertical for Shallow Flows over Rough Beds. *Hydrol. Process.* **37**(2):4820.

Chenevert, M. E. and Dewan, J. T. 2001. A Model for Filtration of Water-Base Mud during Drilling: Determination of Mudcake Parameters. *Petrophysics* **42**(1)237-250.

Deshmukh, V. and Dewangan, S. K. 2022. Review on Various Borehole Cleaning Parameters Related to Oil and Gas Well Drilling. *J. Brazilian Soc. Mech. Sci. Eng*. **44**(5):185.

Elyasi, A., Makarian, E., and Saberi, F. 2023. Fracture Gradient Prediction: Applicable to Safe Drilling and Underground Storage Operations. *Proc*., Seventh International Conferences on Applied Research in Science and Engineering. London, 1-20.

Ershadnia, R., Amooie, M. A, Shams, R., et al. 2020. Non-Newtonian Fluid Flow Dynamics in Rotating Annular Media: Physics-Based and Data-Driven Modeling. *Journal of Petroleum Science and Engineering* **185**(1):106641.

Gamal, H., Bageri, B. S., Elkatatny, S., et al. 2021. Investigating the Alteration of Sandstone Pore System and Rock Features by Role of Weighting Materials. *ACS Omega* **6**(5):4100-4110.

Goshtasbi, K., Elyasi, A., and Naeimipour, A. 2013. 3D Numerical Stability Analysis of Multi-Lateral Well Junctions. *Arab J Geosci* **6**(1):2981-2989.

Hashemi, R., Saberi, F., Asoude, P., et al. 2024. Enhancing Reservoir Zonation through Triple Porosity System: A Case Study. *SPE J*. **29**(6): 3043-3062. SPE-219491-PA

Larki, E., Jaffarbabaei, B., Soleimani, B., et al. 2024. A New Insight to Access Carbonate Reservoir Quality Using Quality Factor and Velocity Deviation Log. *Acta Geophysica* **72**(5):3159-3178.

Li, J., Qiu, Z., Zhong, H., et al. 2022. Effects of Water-Based Drilling Fluid on Properties of Mud Cake and Wellbore Stability. *Journal of Petroleum Science and Engineering* **208**(1):109704.

Liu,Y., Upchurch, E. R., and Ozbayoglu, E. M. 2022. Experimental and Theoretical Studies on Taylor Bubbles Rising in Stagnant Non-Newtonian Fluids in Inclined Non-Concentric Annuli. *Int. J. Multiph. Flow* **147**(1): 103912.

Makarian, E., Abad, A. B. M. N., Manaman, N. S., et al. 2023a. An Efficient and Comprehensive Poroelastic Analysis of Hydrocarbon Systems Using Multiple Data Sets through Laboratory Tests and Geophysical Logs: A Case Study in an Iranian Hydrocarbon Reservoir. *Carbonates and Evaporites* **38**(2):37-50.

Makarian, E., Mirhashemi, M., Elyasi, A., et al. 2023b. A Novel Directional-Oriented Method for Predicting Shear Wave Velocity through Empirical Rock Physics Relationship Using Geostatistics Analysis. *Scientific Reports* **13**(1):19872.

Miao, H., Dokhani, V., Ma, Y., et al. 2023. Numerical Modeling of Laminar and Turbulent Annular Flows of Power-Law Fluids in Partially Blocked Geometries. *Results Eng.* **17**(1):100930.

Mirhashemi, M., Khojasteh, E. R., Manaman, N. S., et al. 2022. Efficient Sonic Log Estimations by Geostatistics, Empirical Petrophysical Relations, and Their Combination: Two Case Studies from Iranian Hydrocarbon Reservoirs. *Journal of Petroleum Science and Engineering* **213**(1):110384.

Nino, L., Gelves, R., Ali, H., et al. 2022. Numerical Determination of Bubble Size Distribution in Newtonian and Non-Newtonian Fluid Flows Based on the Complete Turbulence Spectrum. *Chem. Eng. Sci.* **253**(1): 117543.

Puranik, S. M., Rao, I., R., Sreegowrav, K. R., et al. 2023. Effect of Heat Transfer on Peristaltic Flow of Newtonian Fluid through Eccentric Cylinders. *Case Stud. Therm. Eng.* **45**(1):102912.

Saberi, F., Vashaghian, S., Gyimah, E., et al. 2023. Investigating the Fractures of Asmari Formation as a Geothermal Reservoir with Image Log. *GRC Transactions* **47**(1): 3118-3125.

Saberi, F., Barati Diz, M. B., Kadkhodaie–Ilkhchi, A., et al. 2024a. Creating Capillary Pressure Curves with T2 Data Distribution of NMR Diagram in a Hydrocarbon Field.*SSRN*:1-27

Saberi, F., Asoude, P., and Abdollahzadeh Bina, F. 2024b. Sedimentary Environment, Diagenesis of Sarvak Formation in the Zagros Basin, Iran. Paper presented at the 2nd International Congress on Science, Engineering & New Technologies Hamburg, Germany, 11-13 July.

Saberi, F. and Hosseini-Barzi, M. 2024. Effect of Thermal Maturation and Organic Matter Content on Oil Shale Fracturing. *International Journal of Coal Science & Technology* **11**(1):16.

Salubi, V., Mahon, R., and Oluyemi, G. 2022. The Combined Effect of Fluid Rheology, Inner Pipe Rotation and Eccentricity on the Flow of Newtonian and Non-Newtonian Fluid through the Annuli. *J. Pet. Sci. Eng.* **211**(1): 110018.

Sepehrnoori, K., Proett, M. A., Wu, J., et al. 2005. The Influence of Water-Base Mud Properties and Petrophysical Parameters on Mudcake Growth, Filtrate Invasion, and Formation Pressure. *Petrophysics-The SPWLA J. Form. Eval. Reserv. Descr.* **46**(1):205-235.

Vashaghian, S., Gyimah, E., Olusegun, T., et al. 2024. Petro-Physical Characterization of Lodgepole Formation as a Geothermal Reservoir. *GRC Transactions* **47**(1): 3138-3152.

Vipulanandan, C. and Mohammed, A. 2020. Effect of Drilling Mud Bentonite Contents on the Fluid Loss and Filter Cake Formation on a Field Clay Soil Formation Compared to the API Fluid Loss Method And Characterized Using Vipulanandan Models. *Journal of Petroleum Science and Engineering* **189**(1):107029.

Wu, J., Torres-Verdin, C., Sepehrnoori, K., et al. 2004. Numerical Simulation of Mud-Filtrate Invasion in Deviated Wells. *SPE Reserv. Eval. & Eng.* **7**(2)143-154.

Dai, X., He, L., and J. Chen. 2023. A Method for Matching the Refractive Index and Dynamic Viscosity of Transparent Replicas of Rock for Flow Visualization. *Journal of Visualization* **26**(2): 275-287.

Zanjirabadi, H. R., Saberi, F., Rahimzadeh, B., et al. 2024. Petrology Investigation of Apatite Minerals in the Esfordi Mine, Yazd, Iran. *International Journal of Geological and Environmental Engineering* **18**(4): 118-124.

Fatemeh Saberi is a Ph.D. student in the Department of Geology & Geological Engineering at the University of North Dakota, USA. Her research interests include sedimentology, surface processes, unconventional resources, and the characteristics of carbonate reservoirs.

Sara Vashaghian is a Ph.D. student in the Department of Geology & Geological Engineering at the University of North Dakota, USA. Her research focuses on geology, geothermal energy, and the oil & gas industry. She is affiliated with the University of North Dakota.

Pourya Asoudeh is a master's student in the Department of Geology & Geological Engineering at Shahid Beheshti University, Iran. His research interests include sedimentology, surface processes, unconventional resources, and the characteristics of carbonate reservoirs.

Ahmed E. Radwan is a researcher at the Institute of Geological Sciences, Jagiellonian University, Kraków, Poland, where he specializes in petroleum geosciences, geophysics, environmental geotechnics, geochemistry, and reservoir engineering. He holds a position within the Faculty of Geography and Geology at Jagiellonian University. Radwan's expertise encompasses a broad range of geological and geophysical research, contributing to advancements in petroleum exploration and environmental geotechnics. He is actively engaged in research and publications, with a focus on geosciences and reservoir engineering.